JMEPEG (2008) 17:730–732
DOI: 10.1007/s11665-007-9194-0

1059-9495/$19.00

Residual Stress Analysis of Boronized AISI 1018 Steel by Synchrotron Radiation

J.A. Payne, R.S. Petrova, H.J. White, A. Chauhan, and J. Bai

(Submitted November 6, 2007)

AISI 1018 steel substrates were powder-pack, diffusion boronized at 850 °C for 4 h, followed by air quenching. Optical microscopy in conjunction with color etching was used to obtain the average penetration depth of the iron monoboride layer (9 μm) and the iron diboride layer (57 μm). X-ray diffraction by synchrotron radiation, conducted at the National Synchrotron Light Source in Brookhaven National Laboratory, confirmed the presence of iron monoboride and iron diboride in the boronized plain steel substrates. The $\sin^2 \psi$ technique was employed to calculate the residual stress found in the iron monoboride layer (−237 MPa) and in the substrate layer (−150 MPa) that is intertwined with the needle-like, iron diboride penetration.

Keywords boride layers, boronization, microhardness, residual stress, $\sin^2 \psi$ technique, X-ray powder diffraction

1. Introduction

Boronization is a surface coating applied to ferrous and nonferrous metals that has characteristic properties of high hardness, corrosion resistance, and high temperature oxidation resistance (Ref 1). Many different boronization techniques exist. One of the most commonly employed techniques is powder-pack boronization. This technique was used to boronize the AISI 1018 steel samples used for all tests described in this article.

Powder-pack boronization is a thermochemical treatment in which boron atoms diffuse into and form borides with the particular substrate. The borides formed depend not only on the predominate element in the substrate, but also on the alloying elements. For example, only iron monoboride (FeB) is present in boronized AISI 304 steel, while iron monoboride *and* iron diboride (Fe_2B) are present in boronized AISI 4340 and 1018 steels (Ref 1). In the case of AISI 1018 steel, FeB is found at the surface and Fe_2B is found between the FeB layer and the steel substrate. This is illustrated in Fig. 1, in which the cross section of a boronized AISI 1018 steel sample was color etched to distinguish the FeB layer from the Fe_2B layer. The optical micrograph shown in Fig. 1 also illustrates the needle-like morphology of the constituent boride layers.

J.A. Payne, Department of Materials Science and Engineering, New Jersey Institute of Technology, Newark, NJ 07102-9895; **R.S. Petrova**, Department of Chemistry, New Jersey Institute of Technology, Newark, NJ 07102-9895; **H.J. White** and **A. Chauhan**, Department of Materials Science and Engineering, Stony Brook University, Stony Brook, NY 11794-2275; and **J. Bai**, Department of Materials Science and Engineering, University of Tennessee, Knoxville, TN 37996-2200. Contact e-mail: ssswguy@hotmail.com.

The penetration depth of the boride layers into the substrate can be controlled by diffusion time and temperature. Boride layer thickness displays a parabolic increase with time and a linear increase with temperature (Ref 2). As the boride layer increases in depth there is a corresponding increase in the total thickness of the composite (including the boride layers and substrate) material. However, the increase in thickness of the composite material is comparably very small.

Properties other than the depth of penetration of the boride layers due to varying the time or temperature of diffusion also vary and need to be studied in greater depth. For example, the average grain size of the composite near the substrate/boride layer interface may vary substantially by using different temperatures. Also, it has been shown by Yagyu et al. that the deuterated boronization process causes other elements, particularly carbon, to diffuse toward the substrate/boride layer interface (Ref 3). This phenomenon was also observed (by means of SEM/EDS) for our powder-pack boronization process. Due to the number of variable parameters in the various boronization processes, it is essential that each process be fully characterized in order to find the optimal process for specific applications. In this article, the residual stresses that accrued in the iron monoboride layer and in the near-surface substrate during our powder-pack thermal diffusion boronization process were examined. For reference purposes, the microhardness and layer thicknesses are also given.

2. Experimental Procedure

AISI 1018 steel coupons (38 mm × 19.5 mm × 0.5 mm) were lightly polished with a 600-grit abrasive paper. They were then simultaneously powder-pack boronized for 4 h at 850 °C in a crucible placed in a Thermolyne 48000 box furnace infiltrated with argon. The powder-pack mixture consisted of B_4C, KBF_4, and Al_2O_3. After the four hours of boronization, the crucible and its contents was immediately removed from the furnace and air quenched at room temperature.

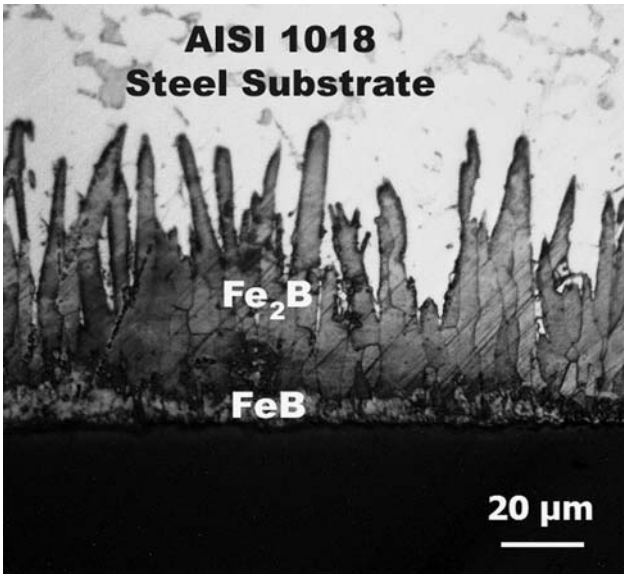

Fig. 1 Optical image of a color-etched cross section of boronized AISI 1018 Steel, displaying the two boride layers and needle-like morphology

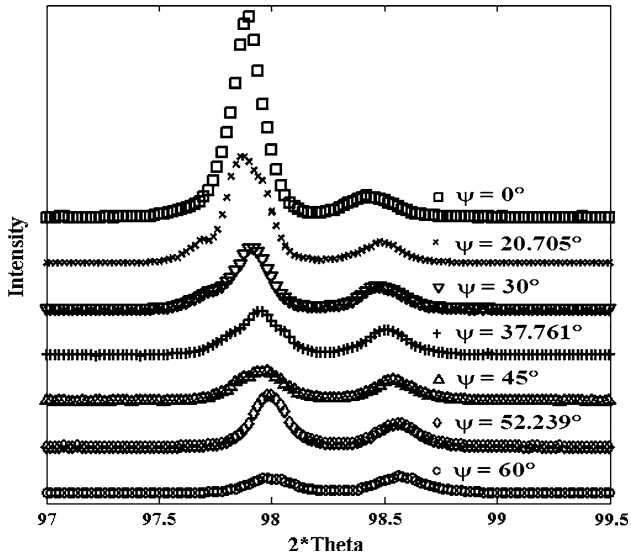

Fig. 2 Variation in 2θ for different tilt angles (First peak: Fe(2 1 1). Second peak: FeB (2 1 2).)

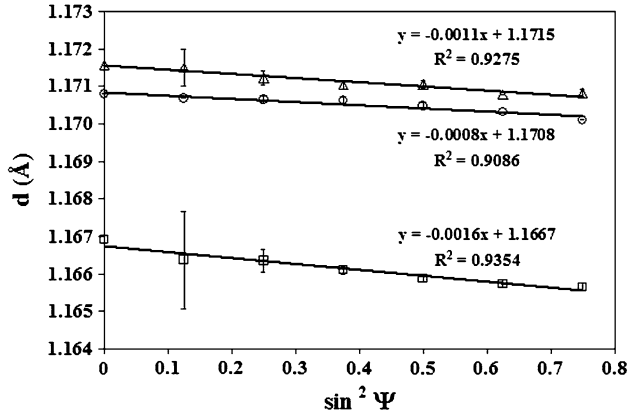

Fig. 3 Atomic planar spacing variation with $\sin^2(\Psi)$ (Data sets: Square: FeB, Circle: Fe uncoated, Triangle: Fe coated.)

Before residual stress measurements were taken, powder X-ray diffraction by a synchrotron radiation source (at Brookhaven National Laboratory) was used to obtain the diffraction peaks of the boronized and unboronized AISI 1018 steel coupons. From these graphs, the (2 1 2) FeB peak and the (2 1 1) Fe peak were chosen to be the peaks used to evaluate the residual stresses. These peaks were chosen due to their relatively high-angle (2θ) proximity on the diffraction spectrum (Ref 4) and because they contained no overlapping peaks.

For reference purposes, the average depth of penetration of the boride peaks and the average coating thickness were obtained by making measurements on the cross section of the samples with a Zeiss Axiotech optical microscope. The microhardness of the coating and the substrate was also found through use of a LECO LM 700 microhardness tester.

3. Results and Discussion

The peak variation from relatively smaller 2θ (twice the angle of the incident X-ray beam) to larger 2θ at increasing ψ (sample tilt angle), as seen in Fig. 2, reveals that compressive stresses are present in the FeB layer and in the substrate of the boronized AISI 1018 steel coupons. By observing the immense and steady decrease in intensity of the Fe (2 1 1) peak from $\psi = 0°$ to $\psi = 60°$, it is evident that the residual stress of the steel is measured very near the coating/substrate interface. This conclusion could also be made simply by observing the large penetration depth of the boride layers. (To increase accuracy, diffraction runs were conducted twice and averaged together to produce the peaks shown in Fig. 2.)

Figure 3 shows the results of the atomic planar spacing, d, versus $\sin^2 \psi$ of FeB and Fe in the boronized specimen and Fe in an unboronized coupon. Since the data display linear characteristics, the $\sin^2 \psi$ technique was employed to calculate the residual stresses (Ref 5-7). The governing equation for this technique is:

$$\frac{d_{\phi\psi} - d_0}{d_0} = \frac{1+\upsilon}{E}\sigma_\phi \sin^2\psi - \frac{\upsilon}{E}(\sigma_{11} + \sigma_{22}),$$

where σ is stress, and υ and E are known values and are Poisson's ratio and Young's modulus, respectively. The angle at which the beam contacts the sample relative to the principle stress directions, 11 and 22, on the surface of the sample, is represented by ϕ. Subscript, 0, indicates that the value is taken at $\psi = 0$. The residual stresses, σ_ϕ, were thus calculated for each data set and are displayed in Table 1. In Table 1, a few other surface-hardening techniques are listed for comparison purposes. It should be noted that these other processes generally have significantly lower microhardnesses.

The average thickness of the coating was found to be 45.3 µm, based on 290 measurements. The average depth of penetration of the FeB layer was found to be 8.6 and 56.9 µm for the Fe_2B layer, based on 116 and 400 measurements, respectively. Microhardness measurements (in units of kg/mm^2) revealed a maximum average Knoop hardness in the coating of 2050 at 13 µm from the surface. Likewise, the maximum

Table 1 Residual stresses found in boronized and unboronized samples

Compound	Residual stress, Pa
FeB	-237×10^6
Fe (coated)	-150×10^6
Fe (uncoated)	-109×10^6
Carburizing (a)	-300×10^6
Plasma nitriding (a)	-425×10^6
Gas sulfonitriding (a)	-375×10^6

(a) Residual stresses on different steel substrates by the processes indicated (Ref 8, 9). The details of these processes are found in (Ref 8, 9)

average Vickers hardness was measured to be approximately 2150 at 25 μm.

4. Conclusion

Coupons of AISI 1018 steel were powder-pack, diffusion boronized at 850 °C for 4 h. X-ray diffraction by synchrotron radiation provided data for the calculation of residual stresses introduced during boronization. For comparison purposes, this calculation (the $\sin^2 \psi$ technique) was also made for unboronized AISI 1018 steel. The iron monoboride layer was found to have a compressive stress of 237 MPa, and the coated iron increased in compressive stress from 109 MPa (uncoated) to 150 MPa. Optical microscopy in conjunction with color etching revealed an average penetration depth of the iron monoboride layer to be 9 and 57 μm in the iron diboride layer. Due to time constraints at the beam line, residual stresses in the Fe_2B layer have not yet been measured, but hopefully will be in the near future.

References

1. R. Petrova and N. Suwattananont, Surface Modification of Ferrous Alloys with Boron, *J. Electron. Mater.*, 2005, **34**(5), p 575–582
2. I. Uslu, H. Comert, M. Ipek, F.G. Celebi, O. Ozdemir, and C. Bindal, A Comparison of Borides Formed on AISI 1040 and AISI P20 Steels, *Mater. Des.*, 2007, **28**(6), p 1819–1826
3. J. Yagyu, N. Ogiwara, M. Saidoh, J. von Seggern, T. Okabe, Y. Miyo, H. Hiratsuka, S. Yamamoto, P. Goppelt-Langer, Y. Aoki, H. Takeshita, and H. Naramoto, Properties of Thin Boron Coatings Formed During Deuterated-Boronization in JT-60, *J. Nucl. Mater.*, 1997, **241**, p 579–584
4. I. Noyan and J. Cohen, *Residual Stress: Measurement by Diffraction and Interpretation*. Springer-Verlag, New York, 1987
5. V. Uglov, V. Anishchik, S. Zlotski, and G. Abadias, The Phase Composition and Stress Development in Ternary Ti-Zr-N Coatings Grown by Vacuum Arc with Combining of Plasma Flows, *Surf. Coat. Tech.*, 2006, **200**(22), p 6389–6394
6. E. Atar, C. Sarioglu, H. Cimenoglu, and E. Kayali, Residual Stresses in (Zr,Hf)N Films (up to 11.9 at.% Hf) Measured by X-ray Diffraction Using Experimentally Calculated XECs, *Surf. Coat. Tech.*, 2005, **191**(2–3), p 188–194
7. U. de Oliveira, V. Ocelik, and J. de Hosson, Residual Stress Analysis in Co-based Laser Clad Layers by Laboratory X-rays and Synchrotron Diffraction Techniques, *Surf. Coat. Tech.*, 2006, **102**(3), p 533–542
8. K. Yatsushiro, M. Hihara, K. Okada, S. Yabuuchi, and M. Kuramoto, Effects of Thermal Cycles on Residual Stress for Nitrided and Sulphonitrided Hot Work Die Steel, *Adv. X-ray Anal.*, 2000, **42**, p 439–450
9. K. Iida and Y. Hirose, The Residual Stress Distribution in Shot Peened Carburized Steel Under Fatigue, 7th Int. Conf. Shot Peen., 1999, p 96–101